Diamond & Related Materials 17 (2008) 2054–2061

Contents lists available at ScienceDirect

Diamond & Related Materials

journal homepage: www.elsevier.com/locate/diamond

Nanostructure, mechanical and tribological properties of reactive magnetron sputtered TiC_x coatings

K. Polychronopoulou [a,b,*], C. Rebholz [b], M.A. Baker [c], L. Theodorou [b], N.G. Demas [a], S.J. Hinder [c], A.A. Polycarpou [a], C.C. Doumanidis [b,d], K. Böbel [e]

[a] Department of Mechanical Science and Engineering, University of Illinois at Urbana-Champaign, Urbana, IL 61801, USA
[b] Department of Mechanical and Manufacturing Engineering, University of Cyprus, 1678, Nicosia, Cyprus
[c] The Surface Analysis Laboratory, Faculty of Engineering and Physical Sciences, University of Surrey, Guildford, GU2 7XH, UK
[d] Department of Mechanical Engineering, Massachusetts Institute of Technology, Cambridge, MA 02139, USA
[e] Plasmatechnology, Business Unit Assembly Systems and Special Machinery, Robert Bosch GmbH, P.O.Box 300220, 70442, Stuttgart, Germany

ARTICLE INFO

Article history:
Received 10 February 2008
Received in revised form 25 June 2008
Accepted 1 July 2008
Available online 11 July 2008

Keywords:
Diamond-like carbon
Nanocrystalline
Sputtering
Tribology

ABSTRACT

This study describes the correlation between microstructure, mechanical and tribological properties of TiC_x coatings (with x being in the range of 0–1.4), deposited by reactive magnetron sputtering from a Ti target in Ar/C_2H_2 mixtures at ~200 °C. The mechanical and tribological properties were found to strongly depend on the chemical composition and the microstructure present. Very dense structures and high hardness, combined with low wear rates and friction coefficients, were observed for coatings with chemical composition close to TiC. X-ray diffraction and X-ray photoelectron spectroscopy analysis, used to evaluate coating microstructure, composition and relative phase fraction, showed that low carbon contents in the coatings lead to sub-stoichiometric nanocrystalline TiC_x coatings being deposited, whilst higher carbon contents gave rise to dual phase nanocomposite coatings consisting of stoichiometric TiC nanocrystallites and free amorphous carbon. Optimum performance was observed for nanocomposite $TiC_{1.1}$ coatings, comprised of nanocrystalline *nc*-TiC (with an average grain size of ~15 nm) separated by 2–3 monolayers of an amorphous *a*-DLC matrix phase.

1. Introduction

Hard and low-friction carbon-based tribological thin solid films and coatings have been the subject of a large amount of research over the last approximately 25 years and cover a wide range of industrial applications such as automotive, forming, punching, plastic moulding, biocompatible implants, and computer hard drives [1]. Hard carbon-based coatings have previously been shown to substantially increase contact fatigue life when applied to steel substrates [2]. Metal-free and metal-containing hard carbon-based coatings have been intensively studied, with the latter reported to possess better adhesion to steel substrates [3].

Transition metal carbides, such as TiC, characterized by short bonds, high hardness, high strength and high thermal and chemical stability, are widely used as wear-resistant materials in, for example, carbide cutting tools [4–13]. One class of metal-containing hard carbon-based coatings are deposited by sputtering pure metal cathodes in inert/hydrocarbon gas mixtures, where coating deposition results from the reaction (at the substrate surface) of the sputtered metal atom flux with the gas phase and ionic and radical hydrocarbon species generated from the glow discharge plasma [5–14]. In the last few years, advances in coating deposition technologies have resulted in the development of supertough wear-resistant coatings, based on nanocrystalline carbides (TiC, WC) in an amorphous diamond-like carbon (DLC) matrix [15,16]. Another approach has been based on metal–metal nanocomposite coatings, promising considerable scope to provide a low coating elastic modulus, while allowing ceramic values of hardness to be achieved. Various studies have shown that physical vapour deposited (PVD) metallic coatings doped with nitrogen, carbon or boron (primarily in supersaturated solid solution) can provide ceramic or near-ceramic hardness, while retaining a low elastic modulus similar to that of the metal substrate component [17,18]. These coatings performed better in laboratory tribological tests compared to (often much harder) ceramic nitride, carbide or boride equivalents, with a correspondingly higher elastic modulus [17,18].

In this study, the synthesis of TiC_x coatings by sputtering a pure Ti cathode in the presence of different Ar/C_2H_2 flow rates is reported. The motivation was to establish a correlation between phase composition/microstructure and tribological behaviour under high contact

* Corresponding author. Department of Mechanical and Manufacturing Engineering, University of Cyprus, 1678, Nicosia, Cyprus. Tel.:+357 22 892772; fax: +357 22 892254.
E-mail address: kyriakip@ucy.ac.cy (K. Polychronopoulou).

0925-9635/$ – see front matter © 2008 Elsevier B.V. All rights reserved.
doi:10.1016/j.diamond.2008.07.007

pressures (mimic realistic conditions) for reactive sputter deposited TiC_x coatings [19–22]. Experimental results for the influence of various amounts of carbon on the structure, mechanical and tribological properties of PVD deposited TiC_x films are presented.

2. Experimental details

TiC_x coatings were deposited onto polished 100Cr6 steel substrates (app. 10 mm×10 mm×3 mm) by reactive pulsed DC magnetron sputtering from a segmented Ti target (5.7 W/cm^2) of 1000 mm× 175 mm×11 mm in argon/acetylene (Ar/C_2H_2) mixtures, using an industrial magnetron sputtering PVD unit with a base pressure of $<10^{-5}$ mbar (10^{-3} Pa) and deposition pressure of 3–3.2×10^{-3} mbar (0.3–0.32 Pa), depending on the C_2H_2 flow rate (varied from 0 to 50 sccm). For coating to substrate adhesion improvement, a 0.2 μm Ti interlayer was deposited prior to TiC_x deposition. The substrate temperature and target to substrate distance were kept constant at ~200 °C and 200 mm, respectively, and no substrate bias voltage was applied. Prior to deposition, the 100Cr6 steel substrates were ultrasonically cleaned in acetone then ethanol and placed on the substrate table of the chamber.

The crystallographic structure and texture of the films were analysed by glancing-angle X-ray diffraction (GAXRD), using CuK_α radiation at an incident angle of 5.0°. The chemical composition of the TiC_x coatings was determined by X-ray photoelectron spectroscopy (XPS), using a VG-Scientific Sigma Probe spectrometer employing a monochromatic AlK_α source and a hemispherical analyser. Argon ion etching was performed at an incident energy of 3 kV and an etch current of ~0.75 μA over an area of approximately 18 mm^2. The XPS high resolution spectra (Ti 2p and C 1 s) were recorded at a 20 eV pass energy and step of 0.2 eV. Quantification was performed using instrument modified Wagner sensitivity factors after a Shirley background subtraction (elemental sensitivity factors were established through analysis of a stoichiometric TiC bulk standard). For bonding information on the DLC phase Raman spectroscopy was used at a laser-wavelength of 515 nm (Ar laser) and a SPEX Triplemate 1877 Triple grating monochromator. The microstructure was investigated using a Philips CM200 transmission electron microscopy (TEM) operated at an incident voltage of 200 keV. Plan view samples were prepared by grinding through the substrate, with the final thinning process involving a Gatan precision ion polisher operating at 5 kV and varying angle below 4°.

Fracture cross-sections of coated samples were prepared for scanning electron microscopy (SEM) morphology and topography studies. Coating roughness and thickness was measured by using a TENCOR P-15 stylus profilometer and a Calotester from CSM (and

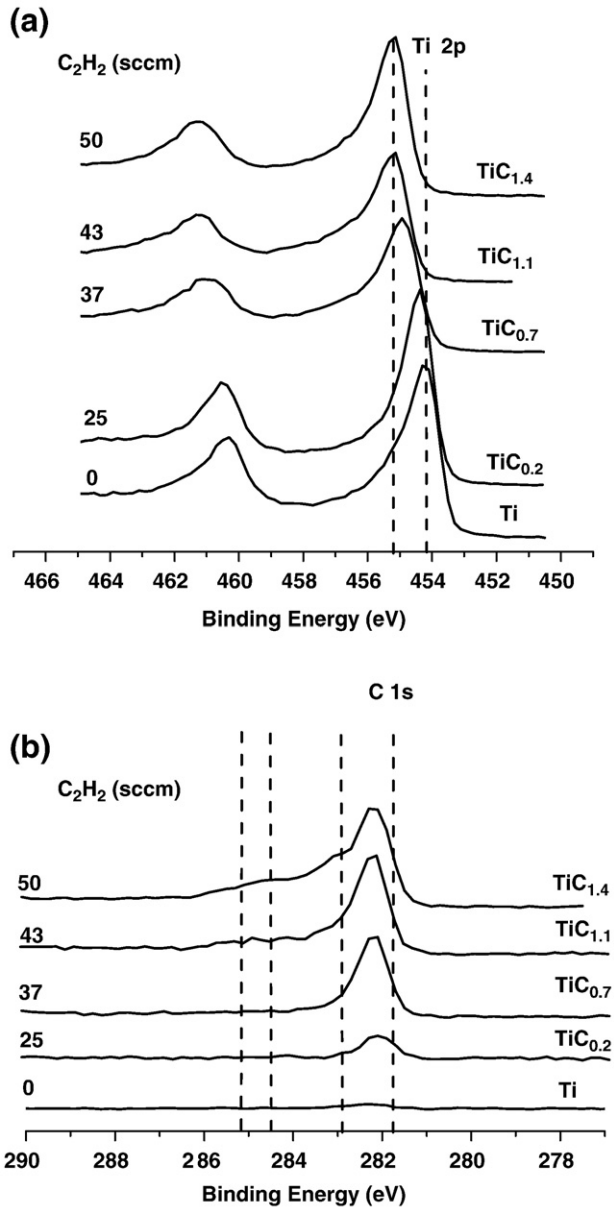

Fig. 2. XPS (a) Ti 2p and (b) C 1s spectra for the TiC_x coatings.

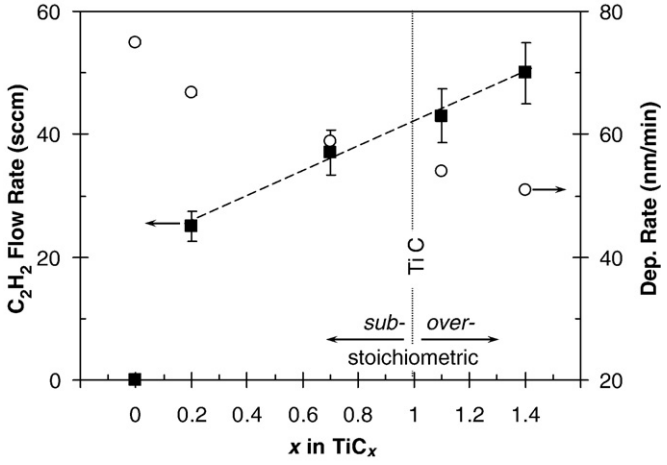

Fig. 1. C_2H_2 flow and deposition rates versus TiC_x composition.

verified by SEM cross-sectional measurements), respectively. Coating adhesion was evaluated according to the Rockwell C hardness test [23], where a coated sample is placed under the Rockwell indenter and a pilot load is applied before the main load (150 kg) is introduced. Coating cracks and/or delamination are compared against a defined adhesion strength quality, with a classification from HF1 to HF6, where HF1 indicates good adhesion, with only radial cracks around the indent, and HF6 indicates poor adhesion. Hardness and reduced elastic modulus values were determined using a Fischerscope H100, equipped with a Vickers indenter, and a Hysitron TriboScope, equipped with a Berkovich indenter. Loads were varied between 10 to 50 mN for the Fisherscope and 3 to 6 mN for the Triboscope, with a sequence of ten indentations at each load.

Ball-on-disc dry sliding experiments were conducted at room temperature (22 °C) and a controlled humidity of 20% using a Standard Tribometer [24]. The sliding velocity was 0.056 m/s at a track radius of 7 mm. For better control of the experimental conditions, namely (a) to maintain a constant contact pressure throughout the whole duration of the experiment, and (b) to only wear the coating, very hard ruby

balls (1.5875 mm in diameter) were used. Using a softer steel ball would result in both wearing of the ball and coating as well as decreasing of the contact pressure with test duration, thus it would have been more difficult to clearly examine the coating performance. A load of 10 N was used corresponding to an initial Hertzian pressure of 2.0 GPa for Ti coatings (deposited at 0 sccm C_2H_2), which showed the lowest hardness. The Hertzian pressure for the hardest coatings (deposited at 43 sccm C_2H_2) was 4.3 GPa. The resulting wear tracks were examined using optical microscopy and SEM and the coating wear volumes were measured by stylus profilometry (TENCOR P-15).

3. Results and discussion

3.1. Coating deposition, composition and relative phase fraction

The coating and phase composition was studied by XPS. TiC_x coatings with $x = 0, 0.2, 0.7, 1.1$ and 1.4 were deposited to a total coating thickness of 2.5 ± 0.2 μm. R_a values were found to be in the range of 70–140 nm, and coatings with a chemical composition close to TiC showed the lowest roughness values, in good agreement with SEM topography studies (see next section). The amount of carbon incorporated in the coatings was a function of the C_2H_2 flow (Fig. 1), and between 25 and 50 sccm an almost linear increase in carbon content in the coatings, together with a decrease in the deposition rate (due to sputter target poisoning effects), was observed. From Fig. 1 it can be seen that stoichiometric TiC is expected to form at a C_2H_2 flow rate of ~42 sccm.

Ti 2p and C 1s core-level spectra of the coatings deposited at different C_2H_2 flow rates are presented in Fig. 2 (a) and (b). The XPS determined coating compositions and relative phase fractions are given in Table 1. The Ti $2p_{3/2}$ peak exhibits a binding energy which progressively increases from 454.1 to 455.2 eV as the C concentration is increased. However, the C 1s carbide peak remains at the same energy (281.9 eV). This is consistent with a progressive change in the TiC_x stoichiometry. As x increases from under-stoichiometric towards stoichiometric and over-stoichimetric values, the nearest neighbour environment of C atoms within TiC_x remains almost unchanged, but for the Ti atoms there is an increasing number of nearest neighbour C atoms, hence the Ti $2p_{3/2}$ peak shifts to higher binding energies. For the $TiC_{0.2}$ coatings (deposited at 25 sccm C_2H_2) its Ti $2p_{3/2}$ peak shifts only slightly from the Ti peak position, which suggests that there is a Ti based phase present in addition to a sub-stoichiometric TiC_x phase.

XPS results for the different TiC_x stoichiometries clearly show that at higher C contents a second C 1s component appears at around 284.8 eV, corresponding to the emergence of *a*-DLC phase in addition to the carbide phase. In Fig. 3, a peak fitted C 1s region for the $TiC_{1.1}$ coatings (deposited at 43 sccm C_2H_2) is given. The peak fit is based on the following peak assignments: bulk TiC at 281.9 eV, C atoms at the edge of the TiC nanocrystallites at 282.9 eV, sp^2 C at 284.5 eV and sp^3 C at 285.2 eV [25–27]. From the peak fits, the TiC_x nanocrystallite stoichiometry and TiC/DLC relative phase fraction was determined [28] (see Table 1). $TiC_{0.2}$ and $TiC_{0.7}$ coatings (deposited at 25 and 37 sccm C_2H_2, respectively) are single phase sub-stoichiometric nanocrystalline TiC_x coatings, whilst $TiC_{1.1}$ and $TiC_{1.4}$ coatings (deposited at 43 and 50 sccm C_2H_2, respectively) are dual phase nanocomposite *nc*-TiC/*a*-DLC coatings with DLC contents of 13 and 20 at.%, respectively. These latter coatings contain a nanocrystalline *nc*-TiC phase which is essentially stoichiometric.

Table 1
Stoichiometry and relative phase fraction for TiC_x coatings deposited at different C_2H_2 flow rates, as obtained from XPS studies

C_2H_2 flow rate (sccm)	Relative phase fractions		TiC_x stoichiometry
	% Carbide	% DLC	
0	–	–	Ti
25	100	0	$TiC_{0.2}$
37	100	0	$TiC_{0.7}$
43	87	13	$TiC_{1.1}$
50	80	20	$TiC_{1.4}$

Sum of O, N and Ar ≤3 at.% in all coatings.

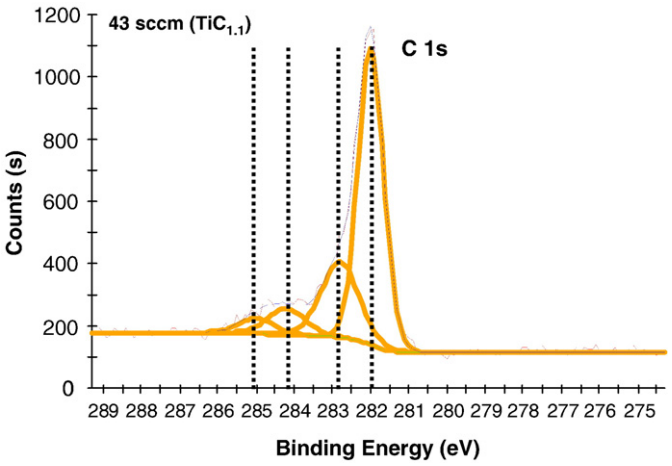

Fig. 3. C 1s peak fitting for the $TiC_{1.1}$ coatings.

The hydrogen content in the coatings under investigation was not studied. Peters et al. [19] deposited Ti-doped hydrogenated DLC coatings using an organometallic CVD-plasma immersion ion processing technique and reported hydrogen contents between 24 and 28 at.%. Meng et al. [29] measured the hydrogen concentration in Ti–C:H coatings deposited by ICP assisted PVD/CVD using Elastic Recoil Detection Analysis (ERDA) and reported hydrogen contents in the 30–37 at.% range.

3.2. Microstructure

Fig. 4 shows the XRD patterns of the TiC_x coatings as deposited on 100Cr6 substrates at different C_2H_2 flow rates (and hence carbon compositions). The standard 2θ positions for fcc (cubic) TiC (JCPDS # 32-1383) have been added to the figure. The TiC (111) peak for the under-stoichiometric $TiC_{0.7}$ coating shows a small (almost negligible) shift to higher angles compared to the JCPDS value. This is in agreement with the

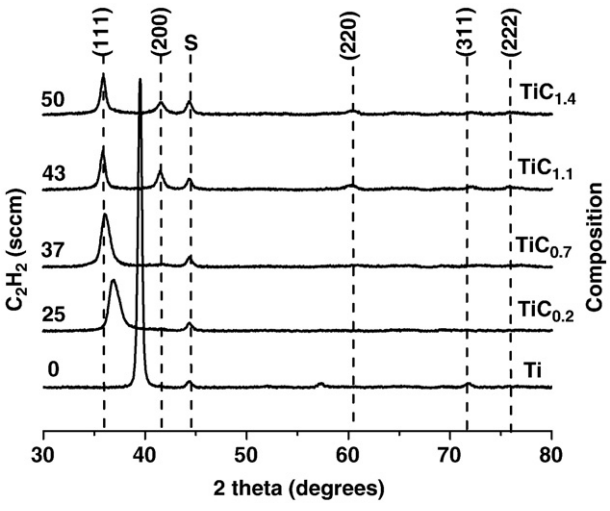

Fig. 4. XRD patterns of the TiC_x coatings.

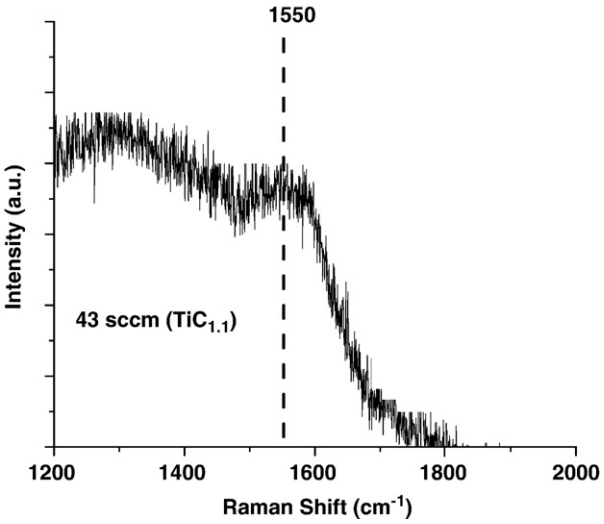

Fig. 5. Raman spectra for the $TiC_{1.1}$ coatings.

theoretical results of Hugosson et al. [30] which showed no significant change in the lattice parameter for TiC_x coatings with stoichiometries in the range $TiC_{0.5}$–$TiC_{1.0}$ [30]. However, there is a substantial shift of the TiC (111) peak to higher angles for the $TiC_{0.2}$ coatings, indicative of lattice parameter changes resulting from the formation of highly sub-stoichiometric TiC_x nanocrystallites. Similar XRD peak shifts have been noted by Inoue et al. [31] and Fujihana [32] for such strongly sub-stoichiometric TiC_x compositions. The sub-stoichiometric coatings also show TiC (111) peak broadening to higher angles, probably due to increased micro-stress. The $TiC_{1.1}$ and $TiC_{1.4}$ coatings exhibit (111) peaks in positions coincident with the JCPDS TiC values as a result of the TiC_x crystallites having essentially stoichiometric compositions (see Table 1). To determine the crystallite size of the coatings, the grain size was determined from the full width half maximum (FWHM) of the X-ray peaks using the Scherrer equation [33]:

$$\text{grain size} = 0.9\lambda/\cos\theta\ \text{FWHM}$$

where λ is the wavelength of the incident radiation and θ the Bragg angle. On the assumption that peak broadening is due to grain size variation only, the FWHM analysis indicated that the TiC_x crystallite size for the $TiC_{1.1}$ coatings was ~15 nm.

Laser Raman Spectroscopy was performed to provide bonding information on the DLC phase. The results for the $TiC_{1.1}$ coatings are given in Fig. 5. It is generally accepted that the relative sp^2 and sp^3 contents are associated with intensities of the Graphitic (G) and Disorder (D) bands in DLC Raman spectra [34]. The G band ranges from 1550 to 1580 cm^{-1} and the D band from 1320 to 1386 cm^{-1}. For the $TiC_{1.1}$ coating both bands are low in intensity due to this coating containing just 13 at.% DLC (predominately sp^2 C). The G band maximum has shifted to lower wavenumbers (1550 cm^{-1}). This shift has been ascribed by Ha et al. [34] and other authors to occur when there is an increase in sp^3 content, hence the a-C phase can be considered to be DLC.

Fig. 6 presents dark field TEM images obtained for the $TiC_{0.7}$ (Fig. 6a) and $TiC_{1.1}$ (Fig. 6b) coatings. The uniform distribution and limited variation in grain size for the TiC nanocrystallites in both coatings is apparent. The average grain sizes for $TiC_{0.2}$ (~4–5 nm) and $TiC_{1.1}$ (~15 nm) are in good agreement with the XRD grain size estimations.

Fig. 7 shows SEM cross-sections obtained for the pure Ti and $TiC_{1.1}$ coatings. The pure Ti coating exhibits a clear columnar microstructure

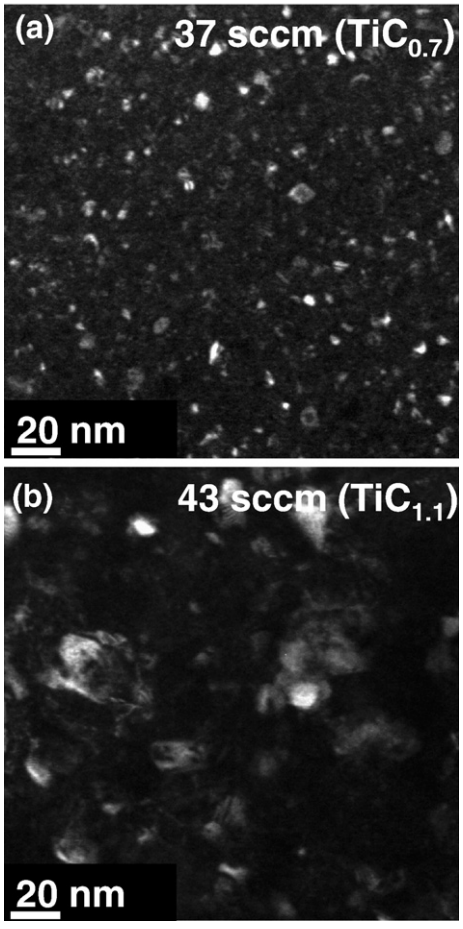

Fig. 6. Dark Field TEM images of (a) $TiC_{0.7}$ and (b) $TiC_{1.1}$ coatings.

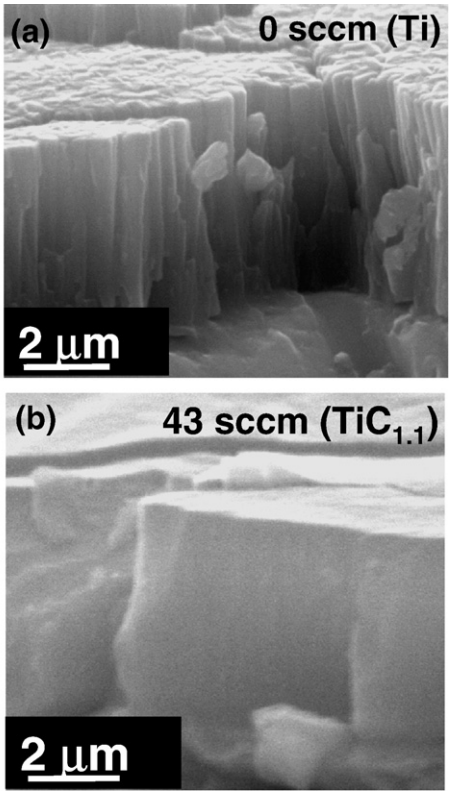

Fig. 7. Scanning electron cross-section micrographs for (a) Ti and (b) $TiC_{1.1}$ coatings.

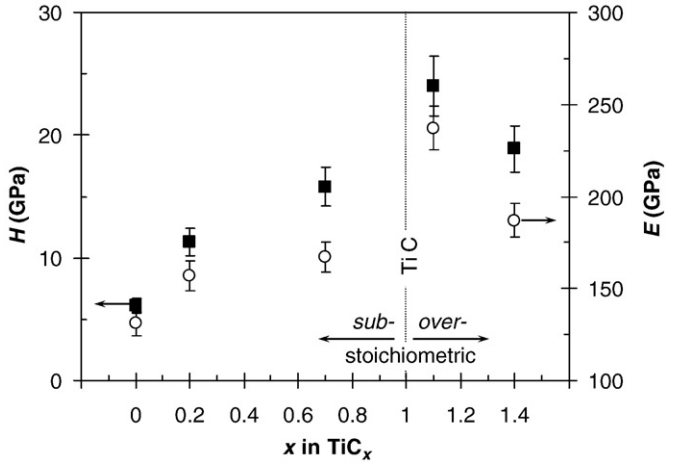

Fig. 8. Hardness and elastic modulus for the TiC_x coatings versus composition.

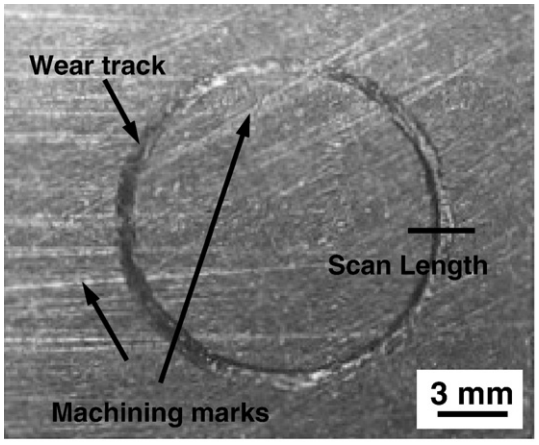

Fig. 10. Optical micrograph of a representative wear track for a TiC_x coated specimen after tribological testing at 10 N, 5000 cycles against ruby–sapphire ball.

whereas the $TiC_{1.1}$ coating exhibits a featureless "glassy" structure. From SEM studies performed on all the coatings it was found that pure Ti coatings and TiC_x coatings with $x \leq 0.7$ exhibited a columnar microstructure. The observed gradual change from a columnar to a non-columnar morphology for TiC_x coatings with $x > 0.7$ is caused initially by a reduction in the TiC_x grain size and then the deposition of a dual nanocomposite *nc*-TiC/*a*-DLC phase.

3.3. Hardness and elastic modulus

Hardness (H) and reduced elastic modulus (E) values for the different TiC_x coatings are plotted in Fig. 8. Very similar H and E values were obtained using the Fisherscope H100 and Hysitron TriboScope (differences ≤ 5%). For Ti coatings (0 sccm C_2H_2), H values of 6 ± 0.5 GPa were measured (similar to bulk Ti values). The relatively low H values can be attributed to the soft metallic character of these coatings as observed in XRD studies. With increasing x in TiC_x, initially a two phase coating of Ti and sub-stoichiometric TiC_x is deposited ($TiC_{0.2}$), then at higher x a single sub-stoichiometric defective TiC_x phase ($TiC_{0.7}$) is formed, leading to progressively increased hardness values. A further increase in x led to a maximum H of 24 ± 2 GPa for $TiC_{1.1}$ coatings, possessing a *nc*-TiC/*a*-DLC phase. The amount of the *a*-DLC phase (13 at.%) corresponds to there being a 2–3 monolayer DLC coverage of the TiC nanocrystallites [35].

Although the nanomechanical properties of TiC coatings may vary depending on the method of deposition and the various deposition parameters, such as substrate bias or carbon content the results obtained in this work are in good agreement with values reported from other researchers. For example, Pei et al. [36] reported H values of between 5.5 and 15.8 GPa for coatings with Ti/C ratio from 0.136 to 0.477, mainly consisting of stoichiometric TiC and sub-stoichiometric $TiC_{0.66}$ phases, and deposited by closed-field unbalanced magnetron sputtering (UBM), while Fang et al. [37] stated values between 20 and 24 GPa for TiC coating deposited by plasma enhanced chemical vapour deposition (PECVD). Peters et al. [19] studied titanium-doped hydrogenated DLC coatings and reported that hardness values

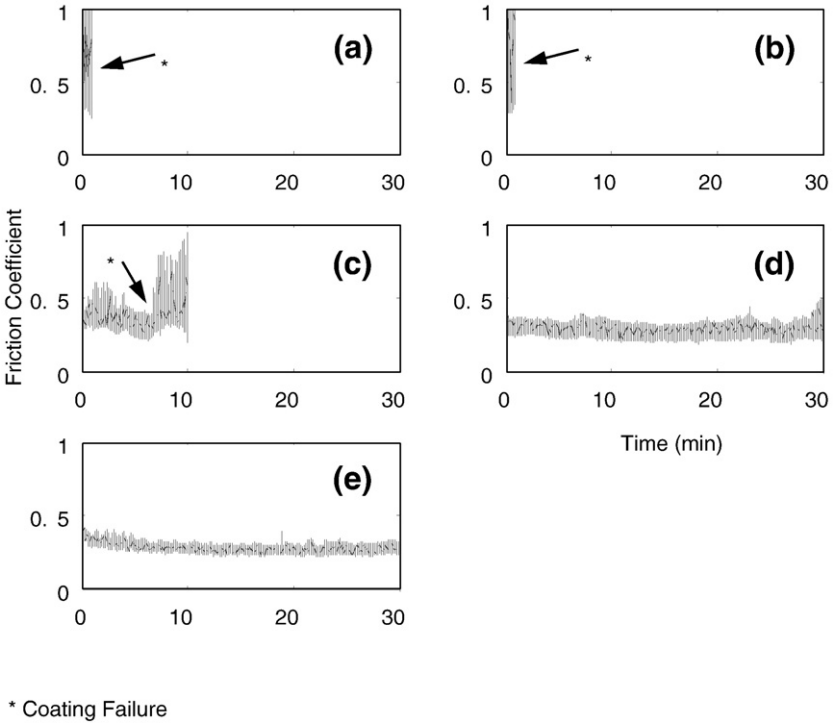

Fig. 9. Friction coefficient plots for the Ti, $TiC_{0.2}$, $TiC_{0.7}$, $TiC_{1.1}$ and $TiC_{1.4}$ coatings.

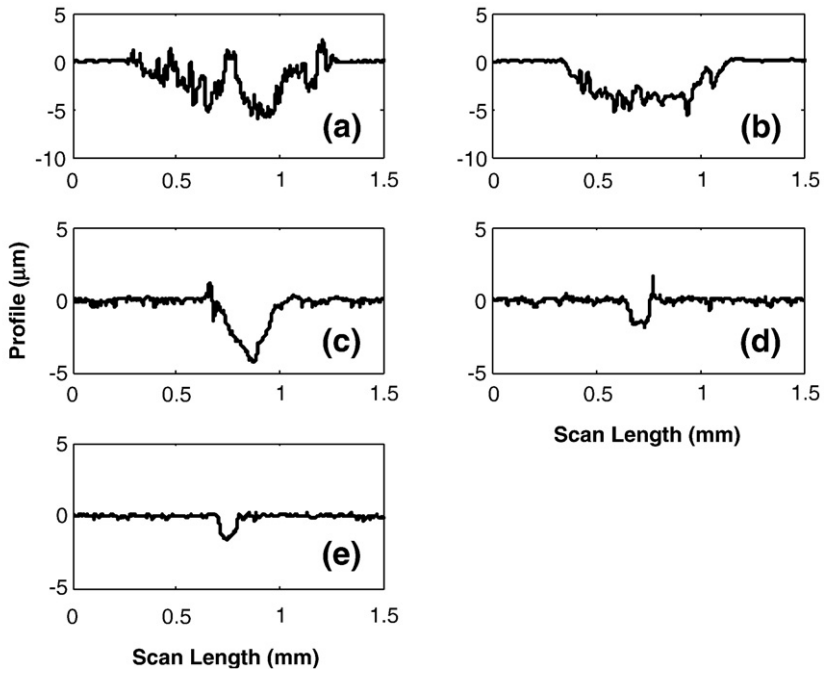

Fig. 11. Profilometric wear scans obtained after tribological tests for the Ti, $TiC_{0.2}$, $TiC_{0.7}$, $TiC_{1.1}$ and $TiC_{1.4}$ coatings.

decreased from 24 GPa (pure DLC coating) to 17 GPa (coating containing 0.4 at.% Ti). Hardness values further decline with increasing Ti content, i.e., hardness of ~7 GPa was achieved for coatings containing 11 at.% Ti. Fig. 8 also clearly shows that with increasing x in TiC_x, i.e. Ti to $TiC_{1.1}$, E increases from 131 ± 7 to 249 ± 12 GPa. For $TiC_{1.4}$ coatings, a decrease in E was observed. The reason for the superior mechanical properties of $TiC_{1.1}$ and $TiC_{1.4}$ coatings, compared to the coatings with $x \leq 0.7$, is probably the smaller TiC crystallite size and presence of DLC, hindering grain boundary sliding [38]. Pei et al. [36] reported E values in the range of 61.3–128.5 GPa for coatings with various Ti/C ratios, and Fang et al. [37] E values of ~270 GPa for their TiC coatings.

The Ti dissolution limit in an a-C matrix is 4–8 at.%, according to ref. [39]. As the Ti composition increases beyond this limit, the volume fraction of TiC_x nanometer sized crystallites embedded within the a-C matrix increases. With increasing TiC_x nanocluster volume fraction, E and H increase significantly. For $TiC_{1.4}$ coatings decreasing H and E values were observed. The decrease in the hardness for TiC_x coatings with $x \geq 1.1$ is mostly associated with the increased a-DLC content. However, increased C incorporation into the TiC lattice, leading to the formation of over-stoichiometric nanocrystallites, may also contribute to the hardness reduction [40].

A good indicator for wear-resistance and film toughness is the H/E ratio [17,18]. For the TiC_x coatings studied here, this ratio was found to increase from 0.05–0.1 with increasing x in TiC_x. Highest H/E values (of the order of 0.1) were found for coatings $TiC_{1.1}$ and $TiC_{1.4}$, deposited at C_2H_2 flow rates from 43–50 sccm, which indicate better elastic behaviour. Ti and $TiC_{0.2}$ exhibit the lowest H/E values, indicating a

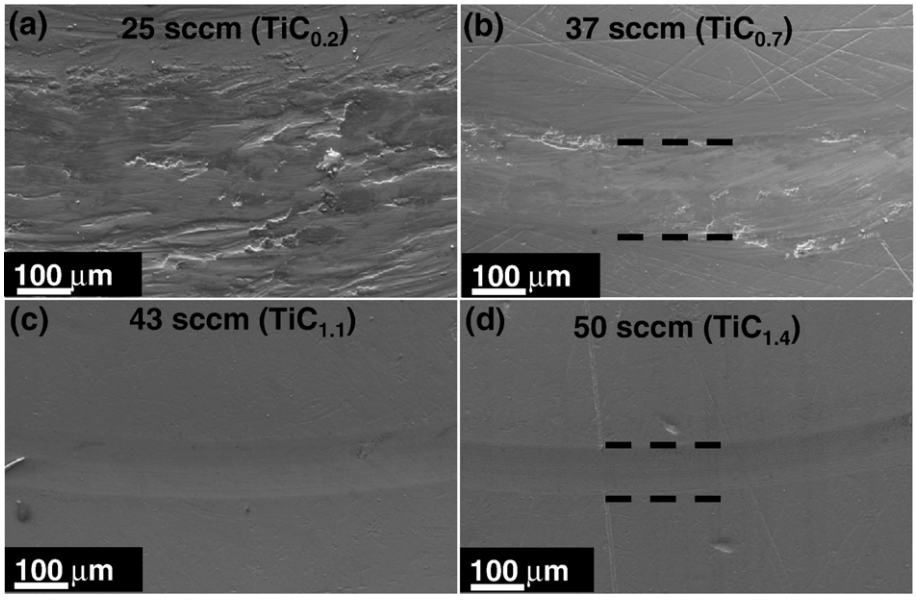

Fig. 12. Scanning electron microphotograph images of the $TiC_{0.2}$, $TiC_{0.7}$, $TiC_{1.1}$ and $TiC_{1.4}$ coated samples after tribological testing.

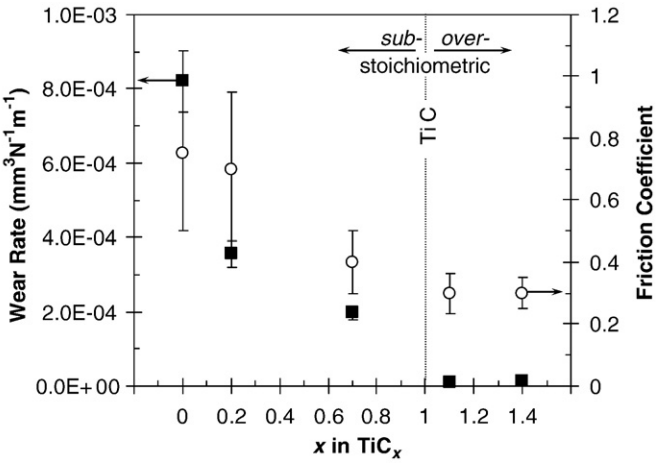

Fig. 13. Effect of the composition on wear rate and friction coefficient for TiC_x coatings.

significantly more plastic behaviour [41]. Independent of the composition, all coatings showed very good adhesion values (HF1-2).

3.4. Tribological performance

Fig. 9 shows the in-situ friction coefficients for all coatings. Fig. 9 (a), (b), (c), (d), (e) and (f) correspond to the Ti, $TiC_{0.2}$, $TiC_{0.7}$, $TiC_{1.1}$ and $TiC_{1.4}$ coatings, respectively. It should be noted that only $TiC_{1.1}$ and $TiC_{1.4}$ coatings (Fig. 9(d) and (e)) were able to withstand the loading conditions for the whole test duration. Testing of all other coated samples had to be stopped prematurely as the friction coefficient increased dramatically, either immediately after the start or during the test, indicating coating failure. For Ti and $TiC_{0.2}$ coatings (Fig. 9(a) and (b), respectively) the tests were stopped immediately after the start, while the $TiC_{0.7}$ coated sample (Fig. 9(c)) was stopped at 10 min, with coating failure occurring after ~7 min.

Fig. 10 shows a micrograph of the wear track of a representative TiC_x coated specimen after 5000 cycles testing (30 min test at 0.056 m/s). Note that the initial machining marks are evident on the sample. Typical profile scans along the wear length for all samples are shown in Fig. 11. As expected, the least amount of wear occurred for $TiC_{1.1}$ and $TiC_{1.4}$ coated samples. The average wear depth over four profilometric measurements was approximately 1.1 μm for $TiC_{1.1}$ and approximately 1.4 μm for $TiC_{1.4}$. The average wear depth for the rest of the samples varied greatly as the coatings were penetrated before the end of the 30-minute test duration. While the average wear depth for these tests does not correspond to coating wear, as in the case for the $TiC_{1.1}$ and $TiC_{1.4}$ coated samples, they can provide an insight as to the type of wear mechanisms involved, as described below.

Fig. 12 shows SEM images of the $TiC_{0.2}$, $TiC_{0.7}$, $TiC_{1.1}$ and $TiC_{1.4}$ coatings, respectively, after tribological testing. As expected, the $TiC_{0.2}$ and $TiC_{0.7}$ coatings (Fig. 12(a) and (b), respectively) show severe damage, while the $TiC_{1.1}$ and $TiC_{1.4}$ coatings (Fig. 12(c) and (d), respectively) are similar and they show minimal damage characteristics. In the case of the $TiC_{0.2}$ coated sample abrasive marks are evident on the surface. These marks are caused by the generation of debris (once the coating acting as a third-body trapped between the very hard ruby–sapphire ball and the coating). Adhesion and material transfer from coating to ruby ball also occurred in this case, determined from examination of the ruby ball counterface. A similar effect, but significantly less pronounced, is evident for the $TiC_{0.7}$ coatings, while the $TiC_{1.1}$ and $TiC_{1.4}$ coatings show mild two-body (ruby ball against coating) abrasion. Note that in all experiments the ruby ball did not show any wear, even though in some tests some minor scratches could be seen. These tribological results are in agreement with the presented microstructure results, where it was shown by TEM and XPS that $TiC_{1.1}$ and $TiC_{1.4}$ nanocomposite coatings have a dual phase microstructure, build of a nanocrystalline TiC phase and an amorphous carbon phase. Additional information for TiC-DLC nanocomposite coatings available from high resolution XPS of the C 1s line revealed that $TiC_{1.1}$ and $TiC_{1.4}$ coatings are dual phase nc-TiC/α-DLC nanocomposites.

The friction coefficient and calculated coating wear rates are presented in Fig. 13. It is observed that the hardest coatings ($TiC_{1.1}$ and $TiC_{1.4}$) exhibited the lowest wear rates and friction coefficients. $TiC_{1.1}$ showed a wear rate of ~1×10^{-5} $mm^3N^{-1}m^{-1}$ and a friction coefficient of ~0.3. TiC_x coatings with $x\leq0.7$ consisting of soft metallic Ti and/or sub-stoichiometric titanium carbides, exhibited lower performance during tribological testing.

Pei et al. [36] reported tribological ball-on-disk experiments with maximum Hertzian contact pressures of 1.5 GPa using 6 mm diameter balls. Sapphire, alumina and bearing steel balls were used with minor differences in the measured friction coefficient values. It should be noted that the contact pressures in this work were much higher, exposing the coating to much more severe conditions. The mean coefficient of friction of one of the coatings reported by Pei et al. [36] was above 0.2, while the rest of the coatings exhibited much lower coefficient of friction values reaching low steady-state values of ~0.05–0.07. Also, a transient behaviour was observed during which the coefficient of friction decreased from an initially high value of about 0.2 at the beginning of sliding until the transition point where steady state was reached. This behavior was attributed to the gradual formation of a transfer film on the counterpart surface during the early stage of the tribological testing. Furthermore, the build-up of this transfer film was dependant on the sliding velocities which varied between 0.1 and 0.5 m/s with less built-up at higher sliding velocities. In the present work, the sliding velocities were similar, however, unlike in Pei et al. [36] where the tribological contact produced evident wear scars on the counterpart, there was no damage on the ruby–sapphire ball counterparts used in this work. There was debris generated during tribological testing, however, a solid transfer film onto the counterpart was not observed. The debris generated was loosely attached onto the surface of the ruby–sapphire ball counterpart and could easily be removed using compressed air. We believe that the reason for the loose debris formation instead of a solid transfer film, is the much higher contact pressures used in this work. Kao et al. [41] investigated the tribological performance of Ti:C–H coatings deposited using UBM. Each test was performed at room temperature under atmospheric pressure and unlubricated conditions using 50 Hz oscillation frequency, a 24 min test period (144 m sliding distance) and a 100 N normal load. Among the investigated coatings, those with high content of carbon (>80%) presented low-friction coefficient (0.29) and low wear depths (2.5 μm). Stüber et al. [27] measured the friction coefficient of TiC–C nanocomposites against 100Cr6 balls of 6 mm diameter, 10 N applied load, 1000 m sliding distance in 25–50% humidity and 23 °C, and reported friction coefficients in the 0.4–0.5 range.

4. Conclusions

In summary, results on the influence of the structure and chemistry on mechanical and tribological properties of TiC_x coatings (with x being in the range of 0–1.4) deposited by reactive magnetron sputtering at different C_2H_2 flow rates have been reported. It can be concluded that:

(1) With increasing carbon content in the coatings the microstructure gradually changes from: Ti + sub-stoichiometric TiC_x, to purely sub-stoichiometric TiC_x and then a nanocomposite *nc*-TiC/*a*-DLC.
(2) The best performing coating was that having a stoichiometry of $TiC_{1.1}$ and a microstructure of stoichiometric TiC nanocrystallites

(with an average grain size of ~15 nm) covered by 2–3 monolayers of DLC. This *nc*-TiC/*a*-DLC coating exhibited the highest hardness (~25 GPa), lowest wear rate ($\sim 1\times10^{-5}$ mm^3 N^{-1} m^{-1}) and friction coefficient (~0.3).

Acknowledgements

The authors gratefully acknowledge financial support from the Cyprus Fulbright Commission, the Air Conditioning and Refrigeration Center, an Industry-University Cooperative Research Center at the University of Illinois at Urbana-Champaign, the Center for Microanalysis of Materials, University of Illinois at Urbana-Champaign, which is partially supported by the U.S. Department of Energy under grant DEFG02-91-ER45439, and FP6 Marie Curie Actions (project EXT-0023899 — *NanoHeaters*) of European Commission.

References

[1] C. Donnet, A. Erdemir, Surf. Coat. Technol. 180/181 (2004) 76.
[2] R. Wei, P.J. Wilbur, F.M. Kustas, J. Tribol. 114 (1992) 298.
[3] L.P. Klages, R. Memming, Mater. Sci. Forum 52/53 (1990) 609.
[4] A. Mani, P. Aubert, F. Mercier, H. Khodja, C. Berthierd, P. Houdy, Surf. Coat. Technol. 194 (2005) 190.
[5] D. Nilsson, F. Svahn, U. Wiklund, S. Högmark, Wear 254 (2003) 1084.
[6] W. Wu, J. Ting, Thin Solid Films 420 (2002) 166.
[7] D. Martinez-Martinez, C. Lopez-Cartes, A. Justo, A. Garcia-Luis, M. Brizuela, JI. Onate, J. Vac. Sci. Technol., A. 23 (2005) 1732.
[8] S. Zahng, XL. Bui, J. Jiang, X. Li, Surf. Coat. Technol. 198 (2005) 206.
[9] A.A. Voevodin, J.S. Jabinski, J. Mater. Sci. 33 (1998) 319.
[10] D. Galvan, Y.T. Pei, J.T.M. DeHosson, Surf. Coat. Technol. 201 (2006) 590.
[11] Y. Hu, L. Li, X. Cai, Q. Chen, P.K. Chu, Diamond Relat. Mater. 16 (2007) 181.
[12] V. Kulikovsky, A. Tarasenko, F. Fendrych, L. Jastrabik, D. Chvostova, F. Franc, L. Soukup, Diamond Relat. Mater. 7 (1998) 774.
[13] T. Tachibana, J.T. Glass, D.G. Thompson, Diamond Relat. Mater. 2 (1993) 37.
[14] K. Bewilogua, H. Dimigen, Surf. Coat. Technol. 61 (1993) 144.
[15] A.A. Voevodin, J.S. Zabinski, Thin Solid Films 370 (2000) 223.
[16] Y.T. Pei, D. Galvan, J.T.M. DeHosson, A. Cavalerio, Surf. Coat. Technol. 198 (2005) 44.
[17] A. Leyland, A. Matthews, Wear 1–2 (2000) 1.
[18] A. Leyland, A. Matthews, Surf. Coat. Technol. 177–178 (2004) 317.
[19] A.M. Peters, M. Nastasi, Surf. Coat. Technol. 167 (2003) 11.
[20] J. Barriga, M. Kalin, K. Van Acker, K. Vercammen, A. Ortega, L. Leiaristi, Wear 261 (2006) 9.
[21] W.P. Hsieh, D.Y. Wang, F.S. Shieu, J. Vac. Sci. Technol., A 17 (1999) 1053.
[22] M. Balden, B.T. Cieciwa, I. Quintana, E. de Juan Pardo, F. Koch, M. Sikora, B. Dubiel, Surf. Coat. Technol. 200 (2005) 413.
[23] H. Jehn (Ed.), Characterisierung dünner Schichten, DIN Fachbericht 39, Beuth Verlag, Berlin–Wien–Zürich, 1993, p. 213, ISBN 3-410-13038-1.
[24] K.M. Lee, A.A. Polycarpou, Wear 259 (2005) 391.
[25] E. Lewin, O. Wilhelmsson, U. Jansson, J. Appl. Phys. 100 (2006) 054303.
[26] M.A. Baker, P. Hammer, Surf. Interface Anal. 25 (1997) 629.
[27] M. Stüber, H. Leiste, S. Ulrich, H. Holleck, D. Schild, Surf. Coat. Technol. 150 (2002) 218.
[28] J. Chastain Jr., R.C. King, Handbook of X-ray Photoelectron Spectroscopy, Physical Electronics, Inc., MN, 1995 ISBN 0-9648124-1-X.
[29] W.J. Meng, R.C. Tittsworth, L.E. Rehn, Thin Solid Films 377 (2000) 222.
[30] H.W. Hugosson, P. Korzhavyi, U. Jansson, B. Johansson, O. Eriksson, Phys. Rev., B 63 (2001) 165116.
[31] S. Inoue, Y. Wada, K. Koterazawa, Vacuum 59 (2000) 735.
[32] T. Fujihana, M. Taniguchi, Y. Okabe, M. Iwaki, Surf. Coat. Technol. 83 (1996) 120.
[33] H.P. Klug, L.E. Alexander, X-ray Diffraction Procedure, Wiley, London, 1988 ISBN 0-471-49369-4.
[34] P.C.T. Ha, D.R. McKenzie, M.M.M. Bilek, S.C.H. Kwok, P.K. Chu, B.K. Tay, Surf. Coat. Technol. 201 (2007) 6734.
[35] M.A. Baker, Surf. Coat. Technol. 201 (2007) 6105.
[36] Y.T. Pei, D. Galvan, J.Th.M. De Hosson, Acta Mater. 53 (2005) 4505.
[37] T.-H. Fang, S.-R. Jian, D.-S. Chuu, Appl. Surf. Sci. 228 (2004) 365.
[38] T. Zehnder, J. Patscheider, Surf. Coat. Technol. 133 (2000) 138.
[39] D. Maier-Schneider, A. Köprülülü, S. Ballhausen Holm, E. Obermeier, J. Micromechanics Microengineering 6 (1996) 436.
[40] W.J. Meng, R.C. Tittsworth, J.C. Jiang, J. Appl. Phys. 88 (2000) 2840.
[41] W.H. Kao, Y.L. Su, S.H. Yao, Vacuum 80 (2006) 604.